

RESEARCH LETTER

10.1002/2017GL076453

Key Points:

- Visso earthquake and nearby faults were destabilized with increasing Coulomb stress induced by pore fluid currents after Amatrice earthquake
- Aftershock migration and clustering are found within the areas of coseismic depressurization and postseismic fluid inflow
- Time delay and location of the Visso earthquake are poroelastically favored by intermediately fractured crust

Supporting Information:

- Supporting Information S1
- Figure S1
- Figure S2
- Figure S3
- Figure S4

Correspondence to:

S. Tung,
sui.tung@sdsmt.edu

Citation:

Tung, S., & Masterlark, T. (2018). Delayed poroelastic triggering of the 2016 October Visso earthquake by the August Amatrice earthquake, Italy. *Geophysical Research Letters*, 45. <https://doi.org/10.1002/2017GL076453>

Received 7 SEP 2017

Accepted 5 FEB 2018

Accepted article online 12 FEB 2018

Delayed Poroelastic Triggering of the 2016 October Visso Earthquake by the August Amatrice Earthquake, Italy

S. Tung¹  and T. Masterlark¹ ¹Department of Geology and Geological Engineering, South Dakota School of Mines and Technology, Rapid City, SD, USA

Abstract Two months after the 2016 Amatrice earthquake (AE), a strong ($\sim M6$) earthquake (Visso earthquake, VE) struck the town Visso, Italy, 20 km north of the AE epicenter. Between these two events, the aftershocks migrated gradually toward to the VE epicenter at a rate of ~ 0.4 km/d, indicating propagation of pore pressure front. We use finite element models to simulate the postseismic fully coupled poroelastic response. The results show that the pore fluid flows (up to 50 nm/s) both horizontally and vertically into the VE hypocenter since the AE and destabilized the area with extra $\sim 70\%$ of Coulomb failure stress. Majority of nearby aftershocks ($>80\%$) tend to cluster within the zones of coseismic depressurization where fluid flow converges. A maximum ΔCFS of ~ 35 kPa is calculated at the VE hypocenter during its rupture by a crustal permeability, $10^{-16} \pm 0.7$ m², suggesting that an intermediately fractured crust allows maximum rupture tendency for the VE during poroelastic fluid recovery.

1. Introduction

Earthquakes interact within the upper crust of the Earth. Extensive work has demonstrated how the changes of lithospheric stress initiated by an earthquake increase or decrease the likelihood of subsequent seismic occurrence in vicinity (Harris & Simpson, 1992; Reasenbergs & Simpson, 1992; Stein, 1999). A preceding earthquake acts as an energy source to perturb the stress field and triggers multiple crustal processes, to which the hypocenters of aftershocks are subjected (Freed, 2007; Marone et al., 1991; Masterlark & Wang, 2002). During the postseismic period, the earthquake-perturbed stress field continuously influences the stability of the surrounding structures (Toda et al., 2005). Coulomb failure stress change (ΔCFS) quantifies the amount of elastic stress transferred from large earthquakes to the proximal fault systems. Its contribution of triggering aftershocks has been recognized in several past events such as the 2015 $M7.8$ Gorkha (Hayes et al., 2015) and the 2009 $M6.3$ L'Aquila earthquake (Walters et al., 2009). In Central Italy, the towns of Amatrice and Visso have been subsequently hit by strong earthquakes ($M \geq 6$) over a time span of 2 months (Chiaraluca et al., 2017). The M_w 6.2 Amatrice earthquake (AE) first took place on 24 August 2016 and was followed by the M_w 6.1 Visso earthquake (VE) on 26 October 2016, only 20 km to the north (Figure 1). Here we investigate the hypothesis that the latter event is favored by the stress redistribution initiated by the former event that broke out 9 weeks earlier.

Transient postseismic mechanisms, such as crustal fluid migration (e.g., Jonsson et al., 2003), afterslip (e.g., Marone et al., 1991), and mantle viscoelastic relaxation (e.g., Bürgmann & Dresen, 2008), interact with the coseismic perturbation of stress fields and hence temporally evolve the ΔCFS experienced by the surrounding faults, in addition to instantaneous dynamic triggering and static stress changes (Convertito et al., 2017). These mechanisms are capable of triggering seismicity (inducing $\Delta CFS > 10$ kPa) or at least advancing or delaying future earthquake occurrence. Their effects are generally location- and time-sensitive and provide an opportunity to quantitatively interpret individual aftershock occurrence. The former two mechanisms are observable in the first few months after an earthquake (Marone et al., 1991; Masterlark & Wang, 2000), whereas the latter endures for decades (Freed & Lin, 2001). Regarding the short time interval (~ 63 days) separating the AE and the VE, our study focuses on how the fluid flow and pore pressure changes initialized by the AE have encouraged the rupture of the VE. The mobilization of pore fluid is activated soon after an earthquake, when a heterogeneous field of pore pressure, Δp , is momentarily built up in an undrained manner within the crustal section of distributed volumetric strain (LaBonte et al., 2009; Wang, 2000). After that, fluid flow modulates the pressure gradients and modifies the stress-pressure field at a rate proportional to the rock hydraulic diffusivity and pressure-gradient steepness (Nur & Booker, 1972). The diffusion of groundwater in the fluid-saturated elastic crust results in time dependence of both the distribution and magnitude of postseismic ΔCFS (Hughes et al., 2010). Wang (2000) casts this transient process into a regime of linear

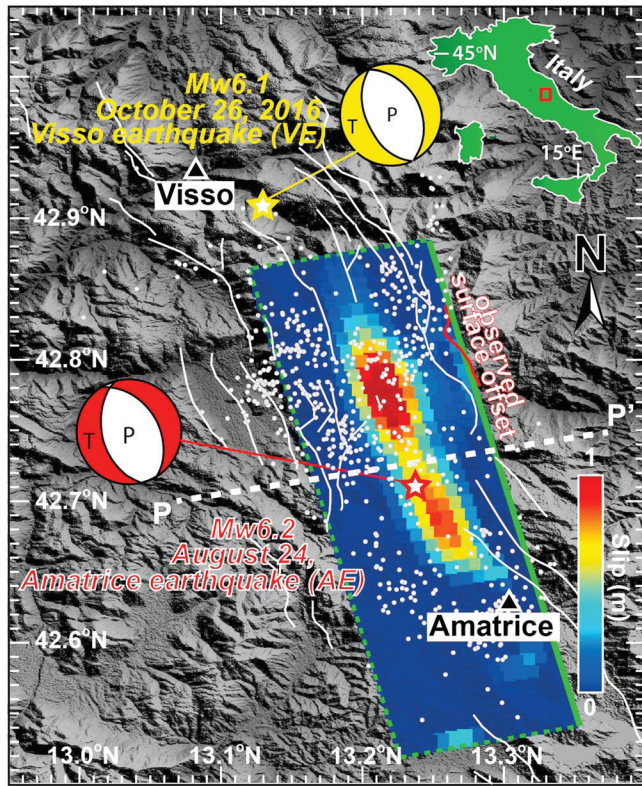


Figure 1. Tectonic map of the August Amatrice earthquake (with colored slip) and the October Visso earthquake. Aftershocks between these two events are plotted as white dots.

poroelasticity describing how the shallow crust couples with pore fluid flow after earthquakes. Poroelastic coupling has been suggested in multiple events including the 2004 $M9$ Sumatra earthquake (Hughes et al., 2010), the 2000 $M6.5$ Iceland earthquake swarm (Jonsson et al., 2003), and the 1992 $M7.3$ Landers earthquake (Masterlark & Wang, 2000). In these cases, the earthquake-induced fluid recovery causes substantial hydraulic pressurization, which led to positive ΔCFS as high as 2 MPa and brought the neighboring structures closer to failure.

In this paper, we study the poroelastic stress coupling between the AE and the following the VE. Fully coupled poroelastic analysis demonstrates how groundwater flux modulates pore pressure and the fault stability near the VE epicenter in a timely manner and determines if this mechanism contributes to its delayed occurrence. Because there are no available data of coseismic groundwater-level changes, we resort to the numerical modeling of postearthquake fluid flow in 3-D finite element models whose dislocation calculation is validated against the customary analytical solution (Okada, 1985) (Figures S1 and S2 and supporting information). We conduct a spatiotemporal analysis of aftershocks against poroelastic coupling and optimize the rock permeability, k , against the occurrence of the VE in the light of the time-dependent variations of Δp and ΔCFS at its hypocenter (e.g., Deng et al., 2016; He & Peltzer, 2010). The results complement the conventional analysis of static ΔCFS with a transient crustal response after the earthquakes and provide insights into the timing and location of aftershocks.

2. Methods

The U.S. Geological Survey National Earthquake Information Center focal plane solution of the VE suggests a fault strike, dip, and rake of 155° , 50° , and -89° , respectively. The probability of frictional failure along the receiver fault of the VE increases with positive ΔCFS (King et al., 1994). King et al. (1994) and Stein (1999) suggest a triggering threshold, $\Delta CFS_{\text{threshold}}$, of positive 10 kPa (King et al., 1994; Stein, 1999) associated with

$$\Delta CFS = \Delta \tau + f(\Delta \sigma + \Delta p) \quad (1)$$

where $\Delta \tau$ denotes shear stress change, $\Delta \sigma$ refers to normal stress change, Δp denotes pore pressure change, and f is the frictional coefficient assumed to be 0.85 (cf. Byerlee, 1978).

We calculate the postseismic transients of Δp and ΔCFS at the VE hypocenter under a fully coupled poroelastic scheme, which is governed by a volumetric strain equation derived from mass conservation and Darcy's law (Wang, 2000):

$$\alpha \frac{\partial \epsilon_{kk}}{\partial t} + S_\epsilon \frac{\partial p}{\partial t} = \frac{k}{\mu_f} \nabla^2 p \quad (2)$$

where α is the Biot-Willis coefficient; t indicates the elapsed time since the loading event (i.e., the AE); $\epsilon_{kk} = \partial u_k / \partial x_k$ is the volumetric strain and subscript k cycles through the orthogonal axis 1, 2, and 3; S_ϵ is the constrained storage coefficient; and k is the intrinsic rock permeability; μ_f is the pore fluid viscosity (Table S1 in the supporting information). It is also constrained by a force equilibrium equation (Detournay & Cheng, 1993; Tung & Masterlark, 2016; Wang & Kumpel, 2003):

$$G \nabla^2 u_i + \frac{G}{(1-2\nu)} \frac{\partial^2 u_k}{\partial x_i \partial x_k} = \alpha \frac{\partial p}{\partial x_i} \quad (3)$$

where G and ν respectively denote the shear modulus and Poisson's ratio which are determined by a local velocity model (Cirella et al., 2012). The Cartesian coordinates and corresponding displacements are denoted as x and u , respectively.

3. Results

3.1. Static Changes of Coulomb Stress

Regarding the stress instantaneously transferred from the AE, the positively stressed zones are overall aligned with the fault strike and form a “Y” shape near the ends of the fault, whereas zones of negative values widely spread over the lateral sides overlapping zones of positive Δp (up to 0.2 MPa) (Figures 2a and 2b). The dumbbell-shaped pressure gradient drives diffusive fluid flow (up to 50 nm/s) toward the lobes of negative Δp near the VE epicenter and the southern fault section near Amatrice (Figure 2b). As such, these coseismic changes subjected the VE hypocenter to a sudden decrease (-15.0 kPa) of pore pressure and an increase (21.0 kPa) of ΔCFS shortly after the AE (Figure 2b).

3.2. Poroelastic Transients of Coulomb Stress

Our poroelastic simulation reveals that the stress field did not remain steady but kept evolving with hydraulic reequilibration following the AE (Figures 2 and S3). Fluid migrated from zones of high pore pressure to those of lower pressure once the pore pressure gradient was established by the AE (Figure 2b). This pressure-gradient-driven mechanism dissipated the gradient retroactively at a rate related to the crustal permeability structure, through which groundwater fluid interacted with the elastic crust and altered the ΔCFS attained by surrounding structures (Figures 2 and S3). The negative Δp (-15.0 kPa) estimated at the VE hypocenter enabled its near-field to become a concentration point to draw pore fluid from the nearby high-pressure zones (Figure 2b). Adopting a representative crustal permeability of 10^{-16} m² (cf. Ingebritsen & Manning, 2010), we simulate subsurface fluid flow (current velocity, v_f up to 50 nm/s) migrating progressively from the lateral positive- Δp zones into those negative- Δp zones near the northernmost and southernmost fault tips (Figure 2b), so that the hypocenter of the VE began to receive an influx of pore fluid soon after the AE. A strong correlation is found between the distribution of converging fluid currents and the aftershock clusters near the town Visso and Amatrice. The vertical profile, AA' further describes that the inflow was not solely contributed by the fluid moving horizontally from the east and the west but also from a region slightly deeper than the focus of the VE beneath the surface (Figures 2b and 2c). The flow rate of this vertical flux near the VE hypocenter was as high as 30 nm/s. In addition, the vertical profile BB' shows how the fluid was directed northward from the near-field of the AE into that of the VE (Figure 2d). These net fluid influxes steadily pressurized the hypocenter of the VE (Figure S3b), reduced the frictional strength of nearby faults, and brought them closer to rupture (Figures 2e and S3a). Meanwhile, ΔCFS at the VE hypocenter was increased by $\sim 70\%$ from 21 kPa of undrained coseismic conditions to 35 kPa at the incidence of the VE (63rd day since the AE) (Figure S3a). On that day, most tectonic structures within 7.5 km from the VE epicenter were destabilized by a positive ΔCFS up to 50 kPa (Figure 2e), as fluid continued flowing into this low-pressure region (Figure 2b). As a result, the aftershock hazard near the town of Visso is dramatically elevated by the fluid migration (Figure 2e). Similar phenomenon is modeled near the center and the southern end of the AE fault where zones of negative ΔCFS dissipated and those of positive ΔCFS dilated (Figures 2a and 2e).

3.3. Spatiotemporal Analysis of Aftershocks and Poroelastic Stress Coupling

The aftershocks taking place between the AE and the VE show a prominent migration of seismicity particularly for those located 15 km away the AE epicenter (Figure 3a). Aftershocks are not intermediately found near the Visso town coseismically stabilized by negative Δp (Figures 2b and 3b). As our simulation shows that the earthquake-induced fluid flow propagates the pore pressure front northward (Figures 2b and 3), the seismicity gradually propagated in a similar direction at a rate of 0.4 km/d. The traveling pressure front gradually restores the Δp from being negative near the Visso town and increases the local ΔCFS beyond the static value (Figures 2a, 2c, 4a, and S3), underlining the combined effects of instantaneous elastic stress changes and the slower fluid diffusion. Aftershocks appear to converge near the epicenter of VE similar to the flow vectors (Figure 3b), highlighting a signature pattern of fluid diffusion. A majority ($>80\%$) of them fall into the quadrant of postseismic pressurization (Figure 4a). A hydraulic diffusivity, D of 1.5 m²/s is found compatible with the migration path, $r = \sqrt{4\pi Dt}$ (where r is the epicentral distance and t is the time elapsed) (Shapiro et al., 2003) (Figure 3a). This migration attains a similar speed to that of nonvolcanic tremors and of induced earthquakes caused by water-injection experiments (Shapiro, Huenges, & Borm, 1997; Tadokoro et al., 2000).

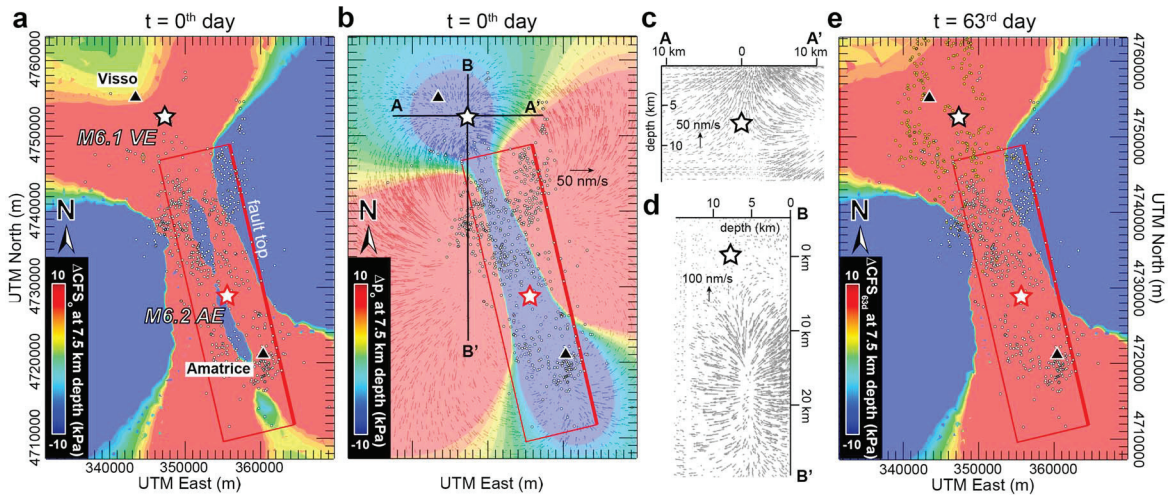


Figure 2. Co/postseismic ΔCFS , Δp , and pore fluid migration. Instantaneous (a) Coulomb stress change, ΔCFS_0 , and (b) pore pressure change, Δp_0 , are calculated at focal depth of the Visso earthquake (VE). (b–d) The arrows show the predicted 3-D field of fluid-flux vectors shortly after the Amatrice earthquake (AE). (e) Poroelastic Coulomb stress changes after 63 days; ΔCFS_{63d} is resolved during the VE rupture. (a, b, and e) The gray dots represent those aftershocks between the AE and the VE, while (e) the yellow dots denote those within 2 days after the VE.

Furthermore, we study the spatial distribution of aftershocks against the temporal poroelastic response in four different regions along the fault (Figure 4c). As mentioned above, majority (83%) of those migrating seismicities near the Visso town (Region 1 in Figure 4a) are subjected to postseismic fluid influx and pressurization. In particular, the VE and ~40% of nearby aftershocks are hydraulically destabilized by an extra ΔCFS of >10 kPa (Figure 4a). Such destabilization is more severe intermediately north of the AE epicenter (Region 2 in Figure 4b), where 87% of aftershocks are favored by fluid coupling and 21% of them (enclosed by cyan dashed line in Figure 4b) achieve the minimum failure threshold of 10 kPa through in situ fluid pressurization. This is very similar to the southernmost aftershock clusters (Region 4 in

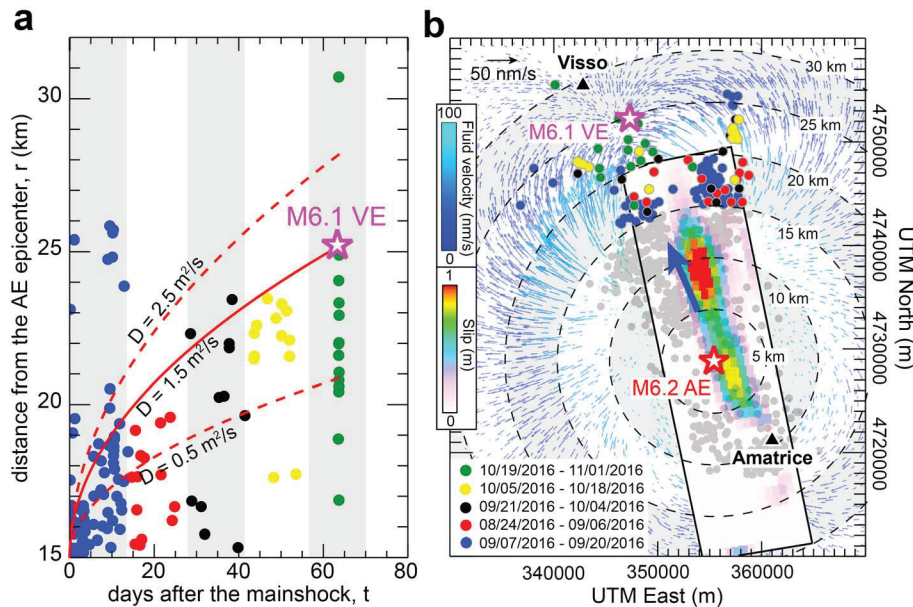


Figure 3. Spatiotemporal analysis of aftershocks between the Amatrice earthquake (AE) and Visso earthquake (VE). (a) Aftershocks located 15 km outside AE epicenter (red star) are color-coded by a 14 day time interval, while those within the 15 km epicentral distance (gray dots). Aftershocks overall migrate northward at a rate of 0.4 km/d ($D \sim 1.5 \text{ m}^2/\text{s}$) and gradually approach VE epicenter (magenta star). (b) Map view of aftershock migration overlaid with coseismic field of flow vector (colored arrows), the earthquake fault (black rectangle), and coseismic slip distribution.

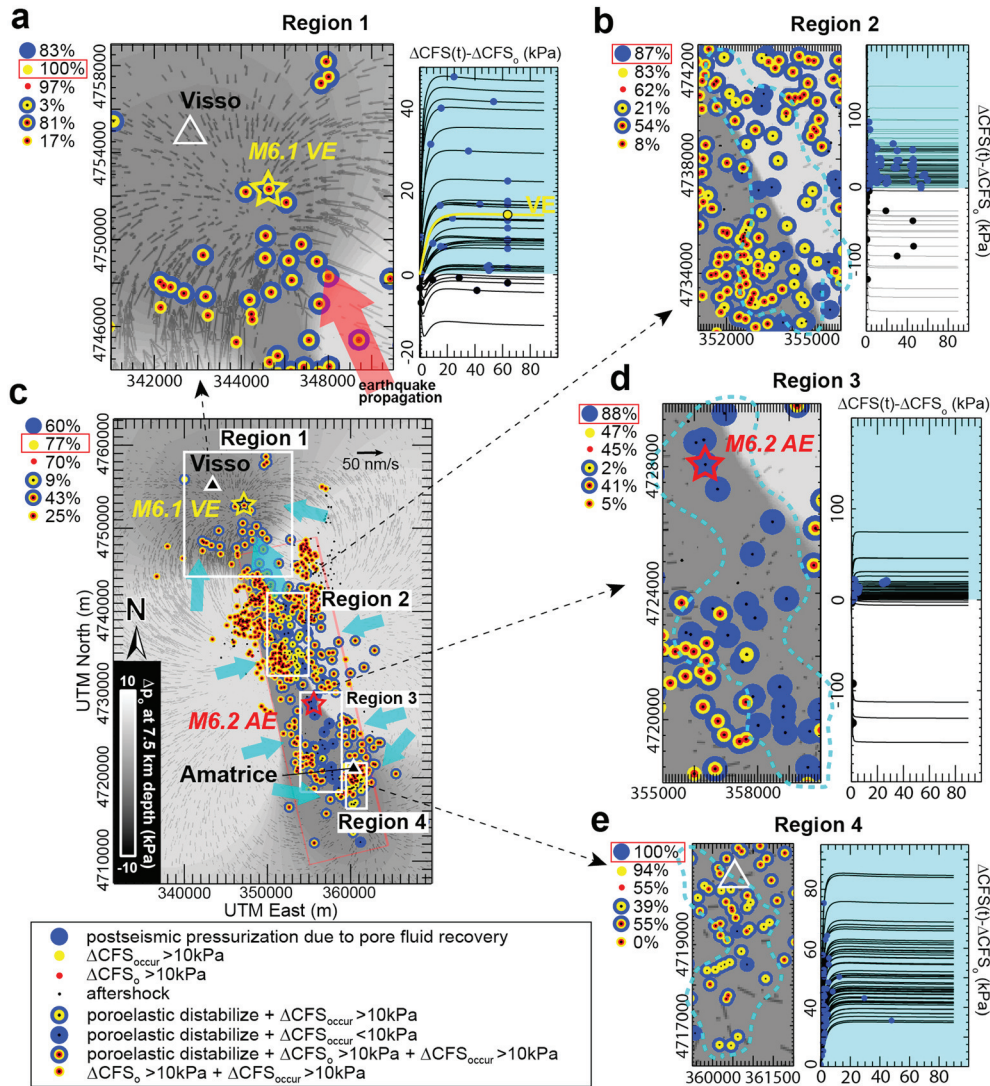


Figure 4. Spatiotemporal analysis of aftershocks coupled with poroelastic stress evolution. The aftershock reception of Coulomb failure stress and fluid-flow coupling are scrutinized in four regions along the Amatrice earthquake rupturing fault. (a) Region 1 reveals a northward earthquake migration (Figure 3) and (>80%) most aftershocks including the Visso earthquake experience increasing pore pressure and $\Delta CFS_0/\Delta CFS_{\text{occur}} > 10\text{kPa}$. (b) Region 2, (c) Region 3, and (d) Region 4 have majority (~90%) of aftershock occurrence (blue dots in both map and cyan-shaded ΔCFS time series) activated by pore fluid coupling. The cyan dashed lines outline those aftershocks that do not have $\Delta CFS_0 > 10\text{kPa}$ but are subjected to postseismic fluid pressurization.

Figure 4d) where nearly all aftershocks are favored by poroelastic coupling and ~40% of them sufficiently reach $\Delta CFS_{\text{threshold}}$ as fluid keeps flowing in. For the area near the AE epicenter (Region 3 in Figure 4d), less than half of the aftershock occurrence is correlated with coseismic $\Delta CFS_0 > \Delta CFS_{\text{threshold}}$, while more than 80% of them gain extra failure tendency due to elevated pore fluid pressure. This analysis shows that static Coulomb stress cannot fully explain the aftershock occurrence as there exists at least ~30% of aftershocks which are not anticipated by ΔCFS_0 , requiring another complementary mechanism to reveal the temporal evolution of near-field failure condition. We found that the poroelastic coupling is compatible with the observations, especially when coming to explain several aftershock clusters (outlined by cyan dashed lines in Regions 2, 3, and 4 of Figure 4) as well as the aftershock sequence migrating toward the Visso town (Figure 3). In particular, more aftershocks are found with $\Delta CFS_{\text{occur}} > \Delta CFS_{\text{threshold}}$ when including the poroelastic coupling effect, which is consistent with the aftershock-stress coupling observed after the nearby 2012 M_w 5.7 Emilia-Romagna, Italy earthquake (Albano et al., 2017) and 2009 $M_6.3$ L'Aquila earthquake (Lucente et al., 2010).

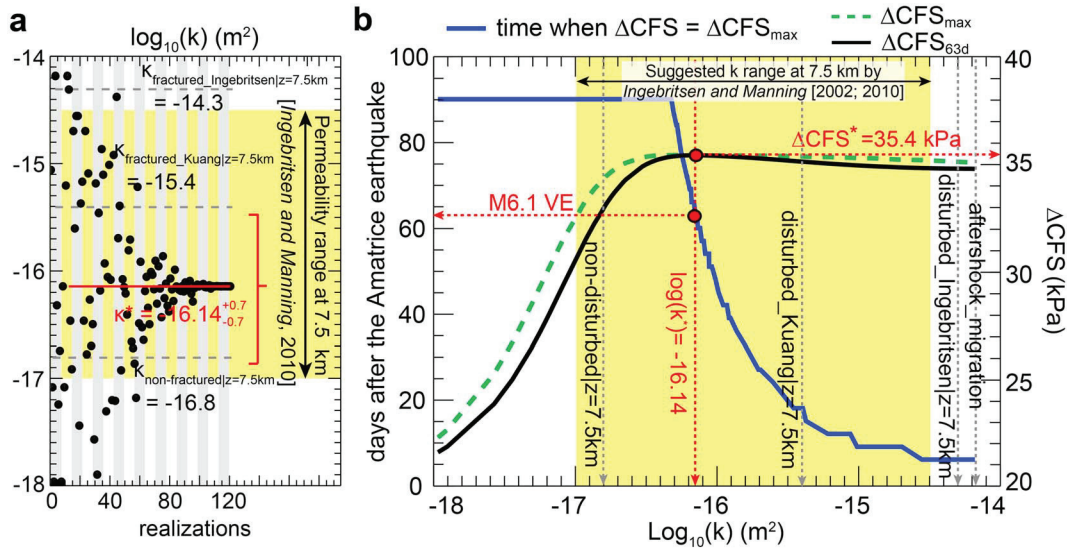


Figure 5. Maximization of ΔCFS at the Visso earthquake (VE) hypocenter by a stochastic permeability search between 10^{-18} and 10^{-14} m². (a) The optimal permeability, $k^* = 10^{-16.1}$ m², enables the VE to be triggered by a maximum ΔCFS^* of 35.4 kPa. The black dots denote the Markov chain Monte Carlo-guided sampling of permeability. (b) Temporal relationship between permeability and ΔCFS evolution experienced by the VE.

4. Discussion and Conclusions

The permeability structure of upper crust is a determining factor regulating the poroelastic mechanism (supporting information and Figure S3). The crustal permeability generally decreases with depth and follows empirical power laws, which is implied by metamorphic and geothermal data (Ingebritsen & Manning, 2010; Manning & Ingebritsen, 1999). As complicated by other factors within the local geological and tectonic environments, the detailed permeability structure of Central Italy is largely unknown (Agosta et al., 2007). However, the overpressurized reservoirs found within the Central Apennines confirm the presence of fluid-saturated crust over the epicentral area and hence accentuate the plausibility of poroelastic triggering mechanism (Terakawa et al., 2010). Provided that these reservoirs are under hydraulic equilibrium (i.e., nontime-dependent) before the AE (cf. Malagnini et al., 2012), we can narrow down the range of permeability values that are in favor of triggering VE through studying the poroelastic coupling process after the AE. We then compare this range to the local structural settings and the corresponding permeability models and interpret the feasibility and manifestation of fluid-induced triggering both in space and time. To begin with, we randomly search for an optimal permeability, k^* , with which a maximum poroelastic change of ΔCFS is attained during the VE rupture (Figures 5 and S4), under a Markov chain Monte Carlo regime. Being insensitive to different frictional coefficients (e.g., 0.4, 0.6, and 0.85), the result shows that the VE experienced the most favorable rupture condition of $\Delta CFS^* = 35.4$ kPa when $k^* = 10^{-16.1}$ m² or 7.94×10^{-17} m² with a 1-sigma uncertainty ranging from 1.48×10^{-17} to 4.27×10^{-16} m² (Figure 5a). This optimal value, k^* , is consistent with the permeability range between $10^{-14.5}$ and 10^{-17} m² at 7.5 km depth, as suggested by Ingebritsen and Manning (2002, 2010) (Figure 5a). This permeability value of k^* is ~2 orders of magnitude smaller than the permeability, $k_{aftershock_migration} = D\Phi\mu_f/K_f = 6.5 \times 10^{-15}$ m² calculated from the observed seismicity migration and a point-source approximation, provided that the porosity, Φ , is 1.1% and pore fluid (water) bulk modulus, K_f , is 2.3 GPa (Antonoli et al., 2005). One possible source of the difference between these estimates is that the former accounts for the heterogeneous field of pore pressure variations, while the latter assumes a point source of pore pressure perturbation. In the former case, the peak ΔCFS^* achieved by the VE fault is ~350% higher than the $\Delta CFS_{threshold}$ and ~70% more than the static value, $\Delta CFS_0 = 21.0$ kPa, demonstrating the fundamental difference between the undrained and drained (poroelastic) response.

We further compare the resolved k^* with the power laws of permeability-depth model (Manning & Ingebritsen, 1999)

$$\log(k) = -14.0 - 3.2 \log(z) \quad (4)$$

where k (m^2) is the permeability at depth z (km). At the 7.5 km depth, the power law yields a permeability of $10^{-16.8}$ or $1.58 \times 10^{-17} \text{ m}^2$, which is ~ 4 times smaller than the optimal permeability, $k^* = 10^{-16.2}$ or $6.92 \times 10^{-17} \text{ m}^2$ (Figure 5a). The higher permeability of k^* is common in seismogenic zones like Central Italy due to the distributed conduits (Agosta et al., 2007; Caine et al., 1996) or the enhanced rates of metamorphic reaction (Ingebritsen & Manning, 2010) within major fault zones. Ingebritsen and Manning (2010) and Kuang and Jiao (2014) update the model for the fractured crust respectively by

$$\log(k_{\text{fractured_Ingebritsen}}) = -11.5 - 3.2 \log(z) \quad (5)$$

$$\log(k_{\text{fractured_Kuang}}) = -8.0 - 19.5 (1 + z)^{-0.45} \quad (6)$$

so that $k_{\text{fractured_Ingebritsen}|z=7.5\text{km}} = 10^{-14.3}$ or $5.0 \times 10^{-15} \text{ m}^2$ and $k_{\text{fractured_Kuang}|z=7.5\text{km}} = 10^{-15.4}$ or $3.59 \times 10^{-16} \text{ m}^2$ (Figure 5a). As $k^* = 10^{-16.2} \text{ m}^2$ is both lower than $k_{\text{fractured_Ingebritsen}|z=7.5\text{km}}$ and $k_{\text{fractured_Kuang}|z=7.5\text{km}}$, it implies that a moderately fractured upper crust would provide the most favorable condition for the VE, which is quite coherent with the active tectonics of the Apennines range experiencing constant seismic activity over the past centuries (Boschi, 2000). Therefore, we confirm that the poroelastic stress coupling is a feasible mechanism for triggering the VE. Moreover, the analysis reveals that the higher the crustal permeability, the earlier the VE hypocenter attains the peak ΔCFS (Figure 5b). The peak ΔCFS occurs between the 6th and the 90th day for permeability between $10^{-16.3}$ and $10^{-14.5} \text{ m}^2$ (Figure 5b). Nonfractured crust ($k = 10^{-16.8} \text{ m}^2$) attains the maximum ΔCFS beyond the 90th day, whereas fractured crust ($k > 10^{-15.4} \text{ m}^2$) allows this to happen before the 20th day (Figure 4c).

We also examine the possibility of two other alternative mechanisms, namely, viscoelastic mantle relaxation and afterslip (rate and state friction) responsible for triggering aftershocks (cf. Bürgmann & Dresen, 2008; Freed, 2007; Marone et al., 1991). Our preliminary analysis of a linear viscoelastic model shows that the viscous behavior of the mantle contributes negligibly ($< 0.075 \text{ kPa}$) toward the ΔCFS at the VE hypocenter over a postseismic period of 63 days, given a viscosity of 10^{-19} or 10^{-24} Pas (Figure S2). Furthermore, very limited postseismic surface displacements ($< 0.1 \text{ m}$, $< 10\%$ of coseismic movements) are observed in the region between the epicenter of the AE and the VE (Figure S2 of Cheloni et al., 2017). This implies that the contribution of frictional afterslip ($\Delta\text{CFS} < 2 \text{ kPa}$) is negligible as compared to $\Delta\text{CFS}_{\text{threshold}}$ and that ($\Delta\text{CFS} \sim 14 \text{ kPa}$) induced by the poroelastic effect for triggering the aftershocks.

In summary, the pore fluid migration modulates pore pressure and promotes significant decrease in fault strength near the epicentral area of the VE. Given a reasonable permeability value, it is very likely that the poroelastic stress coupling was involved in nucleating the VE and caused its delay after the AE. The uncertain tectonic environment such as preseismic stress field and spatially varying rock strength and the contributions of other known/unknown triggering mechanisms infer a certain degree of randomness for aftershock spatio-temporal occurrence (cf. Kagan, 2002; Tormann et al., 2015). However, the nonstochastic nature of the VE timing is characteristically supported by the observable aftershock migration which indicates diffusive transient process. With evidence showing aftershocks tend to cluster and propagate toward the regions of coseismic depressurization where the fault stability is continuously reduced by postearthquake fluid influx, we conclude that a complete assessment of aftershock hazard must include a temporal poroelastic component for predicting those migrating aftershock-prone areas, where another earthquake episode could be triggered.

Acknowledgments

This work is supported jointly by NASA grant NNX17AD96G, NSF grant 1316082, and NASA JPL subcontract 1468758. Academic licensing and technical support for Abaqus software were provided by Dassault Systèmes Simulia Corp. We express our gratitude to Mong-Han Huang for sharing the fault slip model of the AE. The data used are listed in the references, tables, and supplements.

References

- Agosta, F., Prasad, M., & Aydin, A. (2007). Physical properties of carbonate fault rocks, Fucino Basin (Central Italy): Implications for fault seal in platform carbonates. *Geofluids*, 7(1), 19–32. <https://doi.org/10.1111/j.1468-8123.2006.00158.x>
- Albano, M., Barba, S., Solaro, G., Pepe, A., Bignami, C., Moro, M., et al. (2017). Aftershocks, groundwater changes and postseismic ground displacements related to pore pressure gradients: Insights from the 2012 Emilia-Romagna earthquake. *Journal of Geophysical Research: Solid Earth*, 122, 5622–5638. <https://doi.org/10.1002/2017JB014009>
- Antonoli, A., Piccinini, D., Chiaraluca, L., & Cocco, M. (2005). Fluid flow and seismicity pattern: Evidence from the 1997 Umbria-Marche (central Italy) seismic sequence. *Geophysical Research Letters*, 32, L10311. <https://doi.org/10.1029/2004GL022256>
- Bassin, C. (2000). *The current limits of resolution for surface wave tomography in North America*. Eos Trans. AGU.
- Boschi, E. (2000). A 'new generation' earthquake catalogue. *Annals of Geophysics*, 43(4).

- Bürgmann, R., & Dresen, G. (2008). Rheology of the lower crust and upper mantle: Evidence from rock mechanics, geodesy, and field observations. *Annual Review of Earth and Planetary Sciences*, 36(1), 531–567. <https://doi.org/10.1146/annurev.earth.36.031207.124326>
- Byerlee, J. (1978). Friction of rocks. *Pure and Applied Geophysics*, 116(4-5), 615–626. <https://doi.org/10.1007/BF00876528>
- Caine, J. S., Evans, J. P., & Forster, C. B. (1996). Fault zone architecture and permeability structure. *Geology*, 24(11), 1025–1028. [https://doi.org/10.1130/0091-7613\(1996\)024%3C1025:FZAAPS%3E2.3.CO;2](https://doi.org/10.1130/0091-7613(1996)024%3C1025:FZAAPS%3E2.3.CO;2)
- Cheloni, D., De Novellis, V., Albano, M., Antonioli, A., Anzidei, M., Atzori, S., et al. (2017). Geodetic model of the 2016 Central Italy earthquake sequence inferred from InSAR and GPS data. *Geophysical Research Letters*, 44, 6778–6787. <https://doi.org/10.1002/2017GL073580>
- Chiaraluce, L., Di Stefano, R., Tinti, E., Scognamiglio, L., Michele, M., Casarotti, E., et al. (2017). The 2016 Central Italy seismic sequence: A first look at the mainshocks, aftershocks, and source models. *Seismological Research Letters*, 88(3), 757–771. <https://doi.org/10.1785/0220160221>
- Cirella, A., Piatanesi, A., Tinti, E., Chini, M., & Cocco, M. (2012). Complexity of the rupture process during the 2009 L'Aquila, Italy, earthquake. *Geophysical Journal International*, 190(1), 607–621. <https://doi.org/10.1111/j.1365-246X.2012.05505.x>
- Convertito, V., De Matteis, R., & Pino, N. A. (2017). Evidence for static and dynamic triggering of seismicity following the 24 August 2016, MW = 6.0, Amatrice (Central Italy) earthquake. *Pure and Applied Geophysics*, 174, 1–10.
- Deng, K., Liu, Y., & Harrington, R. M. (2016). Poroelastic stress triggering of the December 2013 Crooked Lake, Alberta, induced seismicity sequence. *Geophysical Research Letters*, 43, 8482–8491. <https://doi.org/10.1002/2016GL070421>
- Detournay, E., & Cheng, A. (1993). In E. T. Brown, C. H. Fairhurst, & E. Hoek (Eds.), *Fundamentals of poroelasticity, comprehensive rock engineering, vol 2: Analysis and design methods*. Oxford, UK: Pergamon Press.
- Freed, A. M. (2007). Afterslip (and only afterslip) following the 2004 Parkfield, California, earthquake. *Geophysical Research Letters*, 34, L06312. <https://doi.org/10.1029/2006GL029155>
- Freed, A. M., & Lin, J. (2001). Delayed triggering of the 1999 Hector Mine earthquake by viscoelastic stress transfer. *Nature*, 411(6834), 180–183. <https://doi.org/10.1038/35075548>
- Harris, R. A., & Simpson, R. W. (1992). Changes in static stress on southern California faults after the 1992 Landers earthquake. *Nature*, 360(6401), 251–254. <https://doi.org/10.1038/360251a0>
- Hayes, G. P., Briggs, R. W., Barnhart, W. D., Yeck, W. L., McNamara, D. E., Wald, D. J., et al. (2015). Rapid characterization of the 2015 Mw 7.8 Gorkha, Nepal, earthquake sequence and its seismotectonic context. *Seismological Research Letters*, 86(6), 1557–1567. <https://doi.org/10.1785/0220150145>
- He, J., & Peltzer, G. (2010). Poroelastic triggering in the 9–22 January 2008 Nima-Gaize (Tibet) earthquake sequence. *Geology*, 38(10), 907–910. <https://doi.org/10.1130/G31104.1>
- Huang, M. H., Fielding, E. J., Liang, C., Milillo, P., Bekaert, D., Dreger, D., & Salzer, J. (2017). Coseismic deformation and triggered landslides of the 2016 M_w 6.2 Amatrice earthquake in Italy. *Geophysical Research Letters*, 44, 1266–1274. <https://doi.org/10.1002/2016GL071687>
- Hughes, K. L. H., Masterlark, T., & Mooney, W. D. (2010). Poroelastic stress-triggering of the 2005 M8.7 Nias earthquake by the 2004 M9.2 Sumatra-Andaman earthquake. *Earth and Planetary Science Letters*, 293(3-4), 289–299. <https://doi.org/10.1016/j.epsl.2010.02.043>
- Ingebritsen, S., & Manning, C. (2010). Permeability of the continental crust: Dynamic variations inferred from seismicity and metamorphism. *Geofluids*, 10(1–2), 193–205.
- Ingebritsen, S. E., & Manning, C. E. (2002). Diffuse fluid flux through orogenic belts: Implications for the world ocean. *Proceedings of the National Academy of Sciences*, 99(14), 9113–9116.
- Jonsson, S., Segall, P., Pedersen, R., & Björnsson, G. (2003). Post-earthquake ground movements correlated to pore-pressure transients. *Nature*, 424(6945), 179–183. <https://doi.org/10.1038/nature01776>
- Kagan, Y. Y. (2002). Aftershock zone scaling. *Bulletin of the Seismological Society of America*, 92(2), 641–655. <https://doi.org/10.1785/0120010172>
- King, G. C., Stein, R. S., & Lin, J. (1994). Static stress changes and the triggering of earthquakes. *Bulletin of the Seismological Society of America*, 84(3), 935–953.
- Kuang, X., & Jiao, J. J. (2014). An integrated permeability-depth model for Earth's crust. *Geophysical Research Letters*, 41, 7539–7545. <https://doi.org/10.1002/2014GL061999>
- LaBonte, A. L., Brown, K. M., & Fialko, Y. (2009). Hydrologic detection and finite element modeling of a slow slip event in the Costa Rica prism toe. *Journal of Geophysical Research*, 114, B00A02. <https://doi.org/10.1029/2008JB005806>
- Lucente, F. P., De Gori, P., Margheriti, L., Piccinini, D., Di Bona, M., Chiarabba, C., & Agostinetti, N. P. (2010). Temporal variation of seismic velocity and anisotropy before the 2009 MW 6.3 L'Aquila earthquake, Italy. *Geology*, 38(11), 1015–1018. <https://doi.org/10.1130/G31463.1>
- Malagnini, L., Lucente, F. P., De Gori, P., Akinci, A., & Munafo, I. (2012). Control of pore fluid pressure diffusion on fault failure mode: Insights from the 2009 L'Aquila seismic sequence. *Journal of Geophysical Research*, 117, B05302. <https://doi.org/10.1029/2011JB008911>
- Manning, C., & Ingebritsen, S. (1999). Permeability of the continental crust: Implications of geothermal data and metamorphic systems. *Reviews of Geophysics*, 37, 127–150. <https://doi.org/10.1029/1998RG900002>
- Marone, C. J., Scholz, C., & Bilham, R. (1991). On the mechanics of earthquake afterslip. *Journal of Geophysical Research*, 96, 8441–8452. <https://doi.org/10.1029/91JB00275>
- Masterlark, T. (2003). Finite element model predictions of static deformation from dislocation sources in a subduction zone: Sensitivities to homogeneous, isotropic, Poisson-solid, and half-space assumptions. *Journal of Geophysical Research*, 108(B11), 2540. <https://doi.org/10.1029/2002JB002296>
- Masterlark, T., & Wang, H. (2000). Poroelastic coupling between the 1992 Landers and Big Bear earthquakes. *Geophysical Research Letters*, 27, 3647–3650. <https://doi.org/10.1029/2000GL011472>
- Masterlark, T., & Wang, H. F. (2002). Transient stress-coupling between the 1992 Landers and 1999 Hector Mine, California, earthquakes. *Bulletin of the Seismological Society of America*, 92(4), 1470–1486. <https://doi.org/10.1785/0120000905>
- Motyka, J., Pulido-Bosch, A., Borczak, S., & Gisbert, J. (1998). Matrix hydrogeological properties of Devonian carbonate rocks of Olskuz (Southern Poland). *Journal of Hydrology*, 211(1-4), 140–150. [https://doi.org/10.1016/S0022-1694\(98\)00229-7](https://doi.org/10.1016/S0022-1694(98)00229-7)
- Nur, A., & Booker, J. R. (1972). Aftershocks caused by pore fluid flow? *Science*, 175(4024), 885–887. <https://doi.org/10.1126/science.175.4024.885>
- Okada, Y. (1985). Surface deformation due to shear and tensile faults in a half-space. *Bulletin of the Seismological Society of America*, 75(4), 1135.
- Reasenber, P. A., & Simpson, R. W. (1992). Response of regional seismicity to the static stress change produced by the Loma Prieta earthquake. *Science*, 255(5052), 1687–1690. <https://doi.org/10.1126/science.255.5052.1687>
- Shapiro, S., Patzig, R., Rother, E., & Rindschwentner, J. (2003). Triggering of seismicity by pore-pressure perturbations: Permeability-related signatures of the phenomenon. *Pure and Applied Geophysics*, 160(5), 1051–1066. <https://doi.org/10.1007/PL00012560>

- Shapiro, S. A., Huenges, E., & Borm, G. (1997). Estimating the crust permeability from fluid-injection-induced seismic emission at the KTB site. *Geophysical Journal International*, 131(2), F15–F18. <https://doi.org/10.1111/j.1365-246X.1997.tb01215.x>
- Stein, R. S. (1999). The role of stress transfer in earthquake occurrence. *Nature*, 402(6762), 605–609. <https://doi.org/10.1038/45144>
- Tadokoro, K., Ando, M., & Nishigami, K. y. (2000). Induced earthquakes accompanying the water injection experiment at the Nojima fault zone, Japan: Seismicity and its migration. *Journal of Geophysical Research*, 105, 6089–6104. <https://doi.org/10.1029/1999JB900416>
- Terakawa, T., Zoporowski, A., Galvan, B., & Miller, S. A. (2010). High-pressure fluid at hypocentral depths in the L'Aquila region inferred from earthquake focal mechanisms. *Geology*, 38(11), 995–998. <https://doi.org/10.1130/G31457.1>
- Toda, S., Stein, R. S., Richards-Dinger, K., & Bozkurt, S. B. (2005). Forecasting the evolution of seismicity in southern California: Animations built on earthquake stress transfer. *Journal of Geophysical Research*, 110, B05S16. <https://doi.org/10.1029/2004JB003415>
- Tormann, T., Enescu, B., Woessner, J., & Wiemer, S. (2015). Randomness of megathrust earthquakes implied by rapid stress recovery after the Japan earthquake. *Nature Geoscience*, 8(2), 152–158. <https://doi.org/10.1038/ngeo2343>
- Tung, S., & Masterlark, T. (2016). Coseismic slip distribution of the 2015 Mw7.8 Gorkha, Nepal, earthquake from joint inversion of GPS and InSAR data for slip within a 3-D heterogeneous domain. *Journal of Geophysical Research: Solid Earth*, 121, 3479–3503. <https://doi.org/10.1002/2015JB012497>
- Walters, R., Elliott, J., D'agostino, N., England, P., Hunstad, I., Jackson, J., et al. (2009). The 2009 L'Aquila earthquake (central Italy): A source mechanism and implications for seismic hazard. *Geophysical Research Letters*, 36, L17312. <https://doi.org/10.1029/2009GL039337>
- Wang, H. F. (2000). *Theory of linear poroelasticity: With applications to geomechanics and hydrogeology*. Princeton, NJ: Princeton University Press.
- Wang, R., & Kumpel, H.-J. (2003). Poroelasticity: Efficient modeling of strongly coupled, slow deformation processes in a multilayered half-space. *Geophysics*, 68(2), 705–717. <https://doi.org/10.1190/1.1567241>